Original Full Length Article

Age-related changes in mouse bone permeability

Naiara Rodriguez-Florez[a*], Michelle L. Oyen[b], Sandra J. Shefelbine[c]

[a] Department of Bioengineering, Imperial College London, London SW7 2AZ, UK

[b] Department of Engineering, Cambridge University, Cambridge CB2 1PZ, UK

[c] Department of Mechanical and Industrial Engineering, Northeastern University, Boston MA 02115, USA

*Corresponding author:
Naiara Rodriguez-Florez
Department of Bioengineering, 4.28/2
Imperial College London
London SW7 2AZ, UK
Email: nr211@imperial.ac.uk
Phone: +44 0787 350 9290

Word count: 3479

Keywords: Murine bone, Nanoindentation, Poroelasticity, Permeability, Age

ABSTRACT

The determination of lacunar-canalicular permeability is essential for understanding local fluid flow in bone, which may indicate how bone senses changes in the mechanical environment to regulate mechano-adaptation. The estimates of lacunar-canalicular permeability found in the literature vary by up to eight orders of magnitude, and age-related permeability changes have not been measured in non-osteonal mouse bone. The objective of this study is to use a poroelastic approach based on nanoindentation data to characterize lacunar-canalicular permeability in murine bone as a function of age. Nine wild type C57BL/6 mice of different ages (2, 7 and 12 months) were used. Three tibiae from each age group were embedded in epoxy resin, cut in half and indented in the longitudinal direction in the mid-cortex using two spherical fluid indenter tips (R = 238 μm and 500 μm). Results suggest that the lacunar-canalicular intrinsic permeability of mouse bone decreases from 2 to 7 months, with no significant changes from 7 to 12 months. The large indenter tip imposed larger contact sizes and sampled larger ranges of permeabilities, particularly for the old bone. This age-related difference in the distribution was not seen for indents with the smaller radius tip. We conclude that the small tip effectively measured lacunar-canalicular permeability, while larger tip indents were influenced by vascular permeability. Exploring the age-related changes in permeability of bone measured by nanoindentation will lead to a better understanding of the role of fluid flow in mechano-transduction. This understanding may help indicate alterations in bone adaptation and remodelling.

1. INTRODUCTION

It is well known that bone continuously adapts to its mechanical environment. Previous studies have established that this adaptive response is most likely coordinated by osteocytes, the mechanosensor cells in bone (Burger et al. 1999, Cowin et al. 1995, Han et al. 2004). Osteocyte bodies lie in spaces called lacunae in the mineralized bone matrix and they are connected through small channels termed canaliculi. The mechanical stimulus that drives osteocytes to respond has not been established yet but evidence suggests that fluid flow might perform a major role in cellular excitation. The primary loading-induced fluid motion appears to be through the lacunar-canalicular network, where osteocyte cells sense shear stress due to interstitial fluid movement (Anderson and Knothe Tate 2008, Fritton and Weinbaum 2009, Gardinier et al. 2010, Jacobs et al. 2010, Knothe-Tate 2003). Characterizing lacunar-canalicular network permeability is vital to understand the role of fluid flow in the mechano-transduction mechanism of bone (Anderson et al. 2008, Burger et al. 1999, Lemaire et al. 2012, Price et al. 2011).

Experimentally measuring lacunar-canalicular permeability is challenging due to the heterogeneity of bone and small size of the pores, which is why the first calculations were mainly theoretical. Theoretical estimates based on Biot's poroelasticity theory have given values ranging from 10^{-22} to 10^{-19} m^2 (Gururaja et al. 2005, Wang et al. 1999, Zhou et al. 2008). Finite element models predicted values of 10^{-22} to 10^{-18} m^2 (Lemaire et al. 2012, Smit et al. 2002). Beno et al. (2006) reported values of 10^{-23} - 10^{-19} m^2 with microstructural models of lacunar-canalicular porosity based on geometric data. Stress-relaxation measurements of single osteons measured 10^{-25}-10^{-24} m^2 (Gailani et al. 2009) and compaction of bone gave values of 10^{-23} m^2 (Gardinier et al. 2010). Nanoinentation studies measured values between 10^{-24} to 10^{-21} m^2 for the lacunar-canalicular permeability of equine cortical bone (Galli and Oyen 2009, Oyen 2008, Oyen et al. 2012). Overall, these estimations of lacunar-canalicular

47 permeability range from 10^{-25} to 10^{-18} m^2. This wide range is mainly a result of the fact that
48 vascular and lacunar-canalicular network are interconnected (Fig. 1), making it difficult to
49 separate the contribution of each one to the permeability of bone (Benalla et al. 2012, Jast and
50 Jasiuk 2013, Knothe Tate et al. 2009). In order to isolate effects of lacunar-canalicular
51 permeability independent of vascular permeability, we used nanoindentation.
52 Nanoindentation is a non-destructive way to measure tissue properties of bone and it has
53 recently been used to measure the permeability of hydrated biological tissues (Galli and Oyen
54 2009, Oyen 2008, Oyen et al. 2012). Oyen et al. (2012) found that the values of bone
55 permeability are dependent on the indentation contact size and reported nanoindentation-
56 measured permeability values approximately three orders of magnitude smaller than those
57 given by microindentation. Results from porosity studies also suggest that the probability of
58 measuring specific porosity-ranges in a sample is affected by the inherent structure or density
59 of the interconnected porous network (Jast and Jasiuk 2013, Knothe Tate et al. 2009).
60 Overall, these findings suggest that different indentation contact sizes might measure
61 different hierarchies of bone permeability. In order to investigate this further, spherical
62 indenters of two different radii were used in the current study.

63 The objective of this research was to characterize lacunar-canalicular permeability in young
64 and aged B6 murine bone using a poroelastic approach based on nanoindentation data.
65 Despite the differences between murine and human bone, C57BL/6J (B6) mice are often
66 utilized to explore aspects of age-related bone loss in humans (Halloran et al. 2002, Jilka
67 2013). Unlike human bone, murine bone does not have osteons or Harvesian systems, which
68 is why values of porosity and permeability of human or other animal bone cannot directly be
69 transferred to murine bone. Analyzing age-related changes in mouse bone permeability will
70 provide a better insight into the complex nature of bone permeability and its influence in
71 mechanotransduction.

2. METHODS

Sample preparation

Nine C57BL/6 (B6) female mice of 2, 7 and 12 months, which correspond to young, skeletally mature and old mice respectively, were used for this study. Three right tibiae from each age-group were cleaned of surrounding soft tissue, dried in air for an hour and embedded in epoxy resin (EPOTHIN; Buehler, Lake Bluff, IL, USA). The resin and hardener were mixed and let cool for 15 minutes to increase the viscosity and avoid the infiltration of the resin into the pores. Tibiae were cut at the mid-diaphysis using a low speed diamond saw (Isomet, Buehler GmbH, Germany). The distal sections were cut in cubes and polished using increasing grades of carbide papers (from P800 to P4000).

Nanoindentation

Figure 2 shows the outline of the experimental setup for nanoindentation. Tests were carried out using a TI700 UBI (Hysitron, MN, USA) nanoindenter in load control. The distal halves of the tibiae were glued to a metallic container that covered the stage and indents were done in the longitudinal direction on the tibia mid-diaphyseal cross-sections. Tests were conducted after submerging the specimens in distilled water for at least 15 minutes to fill the pores with fluid. Spherical fluid cell indenter tips of two sizes were used: radius of 238 μm and 500 μm. A trapezoidal loading profile was applied with a rising time of 10 s to a maximum load of 6 mN and a holding time of 30 s. A minimum of ten indents were made on each sample in the mid-cortex around the circumference of the bone. The indents that fell in pores were excluded.

Experimental data from all tests was exported as load-displacement-time (P-h-t) for analysis in MATLAB (The MathWorks, Natick, MA, USA).

3. ANALYSIS

Poroelastic Analysis

The poroelastic analysis proposed by Oyen (2008) and further developed by Galli and Oyen (2009) examines spherical indentation creep responses of hydrated biological materials. During the indentation, the spherical indenter is brought into contact with the surface, pushed into the fully saturated material and retracted, while the applied load, resulting displacement and time are recorded. The rapid local deformation from the indenter causes fluid to be forced out of the material, resulting in pore pressure, which supports part of the applied load. As the fluid leaves the material, pore pressure decreases, resulting in a time-dependent deformation response, which is measured by the nanoindenter. The poroelastic framework assumes that the material has linear isotropic poroelastic behaviour and is fully saturated. Five parameters are required to characterize a poroelastic response: the shear modulus G [N/m^2]; the drained Poisson's ratio v; the undrained Poisson's ratio v_u [ν, 0.5]; the Biot effective stress coefficient α [0, 1]; and the Darcy hydraulic permeability κ [m^4/Ns]. The elastic properties (G and v) correspond to the porous medium considered as a homogeneous linear elastic material. The undrained and drained cases of a fluid-infiltrated porous material represent its limiting behaviors. The undrained response characterizes the condition where the fluid is trapped in the porous solid; while the drained response is related to zero pore pressure (or the pressure corresponding to empty pores).

For an ideal isotropic poroelastic material, the Biot effective stress coefficient α is defined as:

$$\alpha = 1 - \frac{K}{K_s} \qquad [1]$$

where K [N/m^2] is the bulk modulus of the drained material (bone with pores) and K_S [N/m^2] refers to the bulk modulus of the material of the solid skeleton (bone material). The stress

coefficient represents the variation of the fluid volume in a material unit volume due to the volumetric change of the element when loaded under the drained condition.

Darcy hydraulic permeability κ characterizes the flow through the porous elastic skeleton. It is defined as the ratio of the intrinsic permeability k [m^2] to the fluid dynamic viscosity μ (for water μ = 0.001 Pa-s is assumed):

$$\kappa = k/\mu \quad [2]$$

The intrinsic permeability k is related to the porous bone structure only (the connectedness of the porosity and the size and spatial arrangement of the pores), not the fluid in the pores. This is the parameter that will be reported in the current study.

Galli and Oyen (2009) proposed and validated an algorithm to identify these constitutive parameters using a master curve library. The master curves were obtained solving the poroelastic indentation problem utilizing Finite Element modeling for several materials and normalizing their time-displacement indentation response. The non-dimensional displacement h^* is defined as:

$$h^* = \frac{h(t) - h_0(t)}{h_\infty(t) - h_0(t)} \quad [3]$$

where $h(t)$ is the time-dependent displacement of the indenter, h_0 is the indentation depth that corresponds to step-loading conditions, and h_∞ is the indentation depth at $t = \infty$ when the pore pressure field vanishes. These two values can be computed from the elastic solutions (Oyen et al. 2011):

$$h_0(t) = \left(\frac{3P(t)(1-\nu_u)}{8GR^{1/2}}\right)^{2/3} \quad [4]$$

$$h_{\infty}(t) = \left(\frac{3P(t)(1-\nu)}{8GR^{1/2}}\right)^{2/3} \quad [5]$$

where $P(t)$ represents the indentation load and R is the indenter tip radius. The normalized time t^* is given by:

$$t^* = \sqrt{\frac{ct}{Rh(t)}} \quad [6]$$

$\sqrt{Rh(t)}$ represents the contact radius of the indentation. The diffusivity coefficient c is a function of the five constitutive parameters:

$$c = \frac{2\kappa G(1-\nu)(\nu_u - \nu)}{\alpha^2(1-2\nu)^2(1-\nu_u)} \quad [7]$$

Only three constitutive parameters can be identified from spherical indentation data. G, ν, and κ were considered unknown, while the values for α and ν_u were set to 1 (Oyen 2008) and 0.5 (Galli and Oyen 2009, Oyen et al. 2012) respectively. The indenter tip was considered to be impermeable. The percentage of loading ramp analyzed ranged between 1-4%. The poroelastic analysis framework consisted of two optimization steps (Gali and Oyen 2009). The first one occured in the normalized domain (h^*-t^*), where based on initial guesses, the normalized curves were fitted to the master curves in the database. By normalizing the response (eq. 3, 6), the noise of the experimental data can have a greater influence. Hence, the second optimization routine was used to verify that the non-dimensional solution (x^*) gave also the best fit in the dimensional domain. The second routine used the solution from the normalized domain (x^*) as initial guess to fit the curves in the time-displacement domain (h-t) and compute a new dimensional solution (x^d). Both curve fittings were carried out following the non-linear least-squares optimization routine from MATLAB Optimization Toolbox™ as described by Galli and Oyen (2009). Convergence was achieved when the

152 difference between the parameters identified in each domain was negligible ($x^{*} \sim x^{d}$). The final
153 solution (x) contained the values of G, ν, and κ.

154 *Statistical Analysis*

155 The number of indents per age group ranged between 30 and 55 and therefore, unequal
156 sample sizes had to be considered for statistical analysis. Hochberger's GT2 test (post-hoc
157 test) was utilized to compare the means between the three age groups when Levene's test
158 proved homogeneity of variances. If the variances were inhomogeneous, Games-Howell test
159 was used. In order to compare the means of the same bones when indenting with different
160 tips, the Wilcoxon signed-rank test was used. The significant level assumed was 0.05.
161 Statistical analysis was performed using SPSS (v.21, SPSS Inc., Chicago, IL).

162 **4. RESULTS**

163 *Elastic properties*

164 The average values and standard deviations of the elastic properties are summarized in Fig. 3.
165 The shear modulus increased significantly from 2 to 7 months for both indenter tips ($p <$
166 0.001) and then decreased again ($p < 0.001$) in the oldest bones. The 238 μm radius tip
167 measured larger shear modulus for the three ages, but this was significant only for the 7
168 month-old bones ($p = 0.002$). No statistical difference was found in Poisson's ratios between
169 the age groups when indenting the bone with the largest tip. The 238 μm measured smaller
170 Poisson's ratio values for the youngest bones compared to the 7 and 12 months ($p < 0.001$).
171 There were no significant differences between the two tip sizes.

172 *Permeability*

173 Measurements with the small tip revealed that the youngest bones had a larger permeability
174 value ($p < 0.01$) than the older ones but no statistical difference was found between the 7 and

12 month-old bones (Fig. 4). The permeability distribution captured with the two tips is shown in Fig. 5. For the larger radius indents young bones had a narrower range of permeability values (10^{-24} to 5×10^{-23} m^2) while old bones exhibited a broader range (5×10^{-25} to 10^{-21} m^2). An example of the wide range of permeability values captured with the larger tip can be observed in Fig. 6, where displacement-time (h-t) curves of two indents on the same 12 month-old bone result in permeability values that vary three orders of magnitude. This difference in distribution of permeability values was not seen for indents with the smaller tip.

5. DISCUSSION

We used nanoindentation to determine the poroelastic properties of wild type murine tibia as a function of age. The indentations with the small tip revealed a decrease in the lacunar-canalicular permeability from young to skeletally matured tibiae. The 500 μm tip imposed larger contact sizes, which captured both lacunar-canalicular and vascular permeability of bone.

The 238 μm tip showed that lacunar-canalicular permeability decreased from 2 to 7 months with no significant changes from 7 to 12 months (Fig. 4). In vivo tracer transport experiments through the lacunar-canalicular network of rat bone showed that transport becomes more restricted in aged bone due to a more compact mineralized tissue (Knothe Tate et al. 1998). In human cortical bone, porosity of lacunae decreases slightly in older (Wang and Ni, 2003). These findings on osteonal bone seem to follow the same trend of a decrease of lacunar-canalicular permeability with age.

The permeability values we measured (5×10^{-25} to 10^{-21} m^2) are within the range of previous measurements using other experimental methods. Curve fitting of stress-relaxation of single osteons gave lacunar-cannalicular permeability values of 10^{-25}-10^{-24} m^2 for bovine femoral bone (Gailani et al. 2009). This technique cannot be directly employed in murine bone, which

199 does not have osteons. Compaction of intact bone by Gardinier et al. (2010) measured values
200 of 10^{-23} m^2 for lacunar-canalicular permeability of canine metacarpal in situ. Oyen (2008)
201 measured permeability of equine bone using spherical nanoindentation assuming
202 incompressible constituents ($\alpha = 1$ and $\nu_u = 0.5$) and found values of 10^{-24} m^2. In further
203 analysis on different equine bone specimens and using the master curve library together with
204 the poroelastic framework, nanoindentation experiments measured permeability values of 10^{-21}-10^{-23} m^2 (Galli and Oyen 2009, Oyen et al. 2012). In our study, the majority of indents (60-
206 80%) indicated permeability values between 10^{-24} and 5×10^{-24} m^2 for both tips for the three
207 ages evaluated.

208 Though our permeability values are within the range of other studies, quantitative values
209 depend on the testing and analysis methods. The epoxy-embedded bones were dry and then
210 rehydrated before testing, which may have caused changes to the cellular structures inside the
211 lacunae. Anderson et al. (2008) found that permeability decreased at two orders of magnitude
212 when the cellular structure was taken into account in a computational model. This model did
213 not include the effects of lipids and collagen matrix, which decreases permeability a further
214 three orders of magnitude (Wen et al. 2010). Nevertheless, all the samples in the current
215 study underwent the same preparation and testing protocol, and therefore, the effects of
216 freshness are assumed to have affected all the bones in the same manner. The assumptions
217 made in the analysis also influences the values obtained. In our poroelastic approach the
218 values of v_u and α were assigned a priori. The undrained bone was considered incompressible
219 ($v_u = 0.5$), which does not influence the permeability value significantly when compared to v_u
220 < 0.5 (Oyen et al. 2012). The value of $\alpha = 1$ does not influence the elastic properties but since
221 the algorithm identifies k/α^2 from the diffusivity coefficient (eq. 7) the assumed value affects
222 the quantitative value of permeability. Theoretical studies have estimated values of 0.14
223 (Cowin 1999) and 0.15 (Smit et al. 2002) for α in osteonal bone and it has been shown that its

value increases with increasing microporosity or decreasing mineral content (Hellmich and Ulm 2005). The value $\alpha = 1$ was chosen in this study because there are no estimates of what it should be for non-osteonal bone, nor how it changes with age. If $\alpha \neq 1$ was used, all the reported permeability values would differ by a constant value α^2, and thus the age-related trends would not be altered. Overall, the measured values give a first experimental estimate of the lacunar-canalicular permeability of non-osteonal bone.

In order to investigate the influence of the contact size in the measured permeability level, indents made with the 238 μm and 500 μm radius tip were compared. The larger tip imposed larger contact sizes and revealed a wider distribution for the 7 and 12 month-old bones, reaching permeability values as large as 9×10^{-22} m^2 (Fig. 5). These large values were not captured when indenting old bone with the small tip. This difference can be explained by looking at the lacunar and vascular pores of cortical bone (Fig. 7). The indentation contact radius is defined as $a = \sqrt{Rh(t)}$; therefore for an average displacement of ~250 nm the imposed contact diameter was ~ 15 μm for the small tip and ~ 22 μm for the larger tip. The long radius of elliptical lacunae in murine bone measures 1-10 μm with a spacing of ~ 30 μm between lacunae; while the diameter of vascular canals is >10 μm with a vascular spacing of ~100 μm (Carriero et al. 2011, Wang et al. 2005, Schneider et al. 2007, Schneider et al. 2010, Voide et al. 2011). Fig. 7 shows a nano-CT image of a 12 month-old tibia where the long radius of a lacuna is 7.0 μm and the diameter of a vascular canal is 14.2 μm. This suggests that with a larger contact area there is a higher likelihood of indenting a hole or part of a hole. When the indent fell into a pore, the time-displacement curve was either distorted or the displacement limit was exceeded before making contact with the surface. In both cases, this data was excluded from the analysis.

In the current study, the 500 μm tip was able to identify both lacunar-canalicular and vascular permeability, showing a continuum distribution of permeability over three orders of magnitude. These differences in permeability are in accordance with the multi-scale permeability response of equine bone obtained with varying contact sizes: when the contact diameter increased from 6-14 μm to 18 μm, permeability increased almost two orders of magnitude; and it increased three orders of magnitude further when the contact radius reached 200-300 μm (Oyen et al. 2012). In these studies, nanoindentation measured different levels of permeability in a discrete manner; the transition across length scales was not explored further. In the current study, the indents with the 500 μm tip captured this transition and revealed that the permeability distribution was narrower in the youngest bones. This may be a result of the increasing intracortical and cortical porosity with advancing age found in B6 mice femora (Ferguson et al. 2003, Courtland et al. 2013), similar to the increased size of vascular Harvesian canals seen in human bone (Wang and Ni 2003).

The elastic properties derived from the poroelastic analysis did not show such dependence on the indentation contact size and their values were in agreement with published data. Shear modulus increased from young to skeletally mature (2 to 7 months) bone and then decreased in aged mice (12 months). Previous nanoindentation tests on hydrated bone have reported shear moduli of 430-500 MPa (Bembey et al. 2006, Oyen 2008, Oyen et. al 2012). Some studies have measured larger values of shear modulus in dry bone (Bushby et al. 2004, Chang et al. 2011, Lopez-Franco et al. 2011); however, it has been shown that the shear modulus measured by nanoindentation decreases almost an order of magnitude when spherical indentation is used on hydrated bone, in contrast to sharp indentation in dry bone (Rodriguez-Florez et al. 2013). Previous studies have also shown similar age-related changes in elastic properties of B6 murine bone with different measurement techniques at the whole-bone (Brodt et al. 1999, Ferguson et al. 2003, Sommerville et al. 2004) and tissue (Raghavan et al.

2012) level. The drained Poisson's ratios measured in this study are similar to the values obtained by Oyen et al. (2012) and close to the $\nu = 0.3$ often assumed for bone.

This study provides an insight into the changes of lacunar-canalicular permeability of bone with age, as well as a first experimental approximation of lacunar-canalicular permeability of mouse bone. Our results suggest that nanoindentation with varying contact sizes might provide the tool to understand the dual-porosity nature of bone. Recent poroelastic finite-elements models of mouse cortical bone mechanotransduction have shown that the load-repetition response is highly influenced by the assumed value for lacunar-canalicular permeability (Pereira and Shefelbine 2013). The frequency of the load-repetition influences the adaptation of the bone (Kumar et al. 2012, Robling et al. 2002, Warden and Turner 2004). Therefore, it is essential to include accurate experimental lacunar-canalicular permeability values into computational models to explore the influence of fluid flow in bone remodeling and adaptation. Because fluid flow is likely involved in mechanotransduction of the bone's mechanics environment into a cellular mechano-adaptive response, characterizing the permeability of bone may help indicate alterations in mechanoadaptation.

CONFLICT OF INTEREST

None.

ACKNOWLEDGEMENTS

This study has been funded by BBSRC and the Basque Government predoctoral fellowship. Advice given by Daniel G.T. Strange when carrying out the nanoindentation experiments has been of great help.

REFERENCES

294 Anderson, E.J., Knothe Tate, M.L., 2008. Idealization of pericellular fluid space geometry
295 and dimension results in a profound underprediction of nano-microscale stresses imparted by
296 fluid drag on osteocytes. Journal of Biomechanics, 41(8), pp.1736–1746.

297 Bembey, A.K., Oyen, M.L., Bushby, A.J., Boyde, A., 2006. Viscoelastic properties of bone
298 as a function of hydration state determined by nanoindentation. Philosophical Magazine,
299 86(33-35), pp.5691–5703.

300 Benalla, M., Cardoso, L. and Cowin, S.C., 2012. Analytical basis for the determination of the
301 lacunar–canalicular permeability of bone using cyclic loading. Biomechanics and Modeling
302 in Mechanobiology, 11(6), pp.767–780.

303 Beno, T., Yoon, Y-J., Cowin, S.C., Fritton, S.P., 2006. Estimation of bone permeability using
304 accurate microstructural measurements. Journal of Biomechanics, 39(13), pp.2378–2387.

305 Brodt, M.D., Ellis, C.B., Silva, M.J., 1999. Growing C57Bl/6 Mice Increase Whole Bone
306 Mechanical Properties by Increasing Geometric and Material Properties. Journal of Bone and
307 Mineral Research, 14(12), pp.2159–2166.

308 Burger, E.H. and Klein-Nulend, J., 1999. Mechanotransduction in bone—role of the lacuno-
309 canalicular network. The FASEB Journal, 13(9001), pp.S101–S112.

310 Bushby A.J., Ferguson V. L., Boyde A., 2004. Nanoindentation of bone: comparison of
311 specimens tested in liquid and embedded in polymethylmethacrylate. Journal of Materials
312 Research, 19(1), pp. 249–259

313 Carriero A., Doube M., Levchuk A., Schneider P., Muller R., Shefelbine S.J., 2011. Cortical
314 tissue porosity of brittle osteogenesis imperfecta bone. Transactions of the annual meeting of
315 the ORS, [Boston] Orthopaedic Research Society; Long Beach, CA, USA.

316 Chang, Y.-T., Chen, C.-M., Tu, M.-Y., Chen, H.-L., Chang, S.-Y., Tsai, T.-C., Wang, Y.-T.,
317 Hsiao, H.-L., 2011. Effects of osteoporosis and nutrition supplements on structures and
318 nanomechanical properties of bone tissue. Journal of the Mechanical Behavior of Biomedical
319 Materials 4(7), pp.1412–1420.

320 Courtland, H.-W., Kennedy, O.D., Wu, Y., Gao, Y., Sun, H., Schaffler, M.B., Yakar, S.,
321 2013. Low levels of plasma IGF-1 inhibit intracortical bone remodeling during aging. Age
322 (Dordrecht, Netherlands) 35(5), pp.1691–1703.

323 Cowin, S.C., Weinbaum, S., Zeng, Y., 1995. A case for bone canaliculi as the anatomical site
324 of strain generated potentials. Journal of Biomechanics, 28(11), pp.1281–1297.

325 Cowin, S.C., 1999. Bone poroelasticity. Journal of Biomechanics, 32(3), pp.217–238.

326 Ferguson, V.L., Ayers, R.A., Bateman, T.A., Simske, S.J., 2003. Bone development and age-
327 related bone loss in male C57BL/6J mice. Bone, 33(3), pp.387–398.

328 Fritton, S.P. and Weinbaum, S., 2009. Fluid and Solute Transport in Bone: Flow-Induced
329 Mechanotransduction. Annual Review of Fluid Mechanics, 41(1), pp.347–374.

330 Gailani, G., Benalla, M., Mahamud, R., Cowin, S.C., Cardoso, L., 2009. Experimental
331 determination of the permeability in the lacunar-canalicular porosity of bone. Journal of
332 Biomechanical Engineering, 131(10), p.101007.

333 Galli, M. and Oyen, M.L., 2009. Fast identification of poroelastic parameters from
334 indentation tests. CMES: Computer Modeling in Engineering and Sciences, 48(doi:), pp.241–
335 270.

336 Gardinier, J.D., Townend, C.W., Jen, K-P., Wu, Q., Duncan, R.L., Wang, L., 2010. In situ
337 permeability measurement of the mammalian lacunar–canalicular system. Bone, 46(4),
338 pp.1075–1081.

339 Gururaja, S., Kim, H.J., Swan, C.C., Brand, R.A., Lakes, R.S., 2005. Modeling deformation-
340 induced fluid flow in cortical bone's canalicular-lacunar system. Annals of Biomedical
341 Engineering, 33(1), pp.7–25.

342 Halloran, B.P., Ferguson, V.L., Simske, S.J., Venton, L.L., Majumdar, S., 2002. Changes in
343 Bone Structure and Mass With Advancing Age in the Male C57BL/6J Mouse. Journal of
344 Bone and Mineral Research, 17(6), pp.1044–1050.

345 Han, Y., Cowin, S.C., Schaffler, M.B., Weinbaum, S., 2004. Mechanotransduction and strain
346 amplification in osteocyte cell processes. Proceedings of the National Academy of Sciences
347 of the United States of America, 101(47), pp.16689–16694.

348 Hellmich, C., Ulm, F.-J., 2005. Drained and Undrained Poroelastic Properties of Healthy and
349 Pathological Bone: A Poro-Micromechanical Investigation. Transport in Porous Media 58(3),
350 pp.243–268.

351 Jacobs, C.R., Temiyasathit, S., Castillo, A.B., 2010. Osteocyte Mechanobiology and
352 Pericellular Mechanics. Annual Review of Biomedical Engineering, 12(1), pp.369–400.

353 Jast, J. and Jasiuk, I., 2013. Age-related changes in the 3D hierarchical structure of rat tibia
354 cortical bone characterized by high-resolution micro-CT. J. Journal of Applied Physiology,
355 114(7), pp.923–933.

356 Jilka, R.L., 2013. The Relevance of Mouse Models for Investigating Age-Related Bone Loss
357 in Humans. The Journals of Gerontology Series A: Biological Sciences and Medical
358 Sciences.

359 Knothe Tate, M.L., Niederer, P., Knothe, U., 1998. In vivo tracer transport through the
360 lacunocanalicular system of rat bone in an environment devoid of mechanical loading. Bone
361 22(2), pp.107–117.

362 Knothe Tate, M.L., 2003. 'Whither flows the fluid in bone?' An osteocyte's perspective.
363 Journal of biomechanics, 36(10), pp.1409–1424.

364 Knothe Tate, M.L., Steck, R., Anderson, E.J., 2009. Bone as an inspiration for a novel class
365 of mechanoactive materials. Biomaterials 30(2), pp.133–140.

366 Kumar Chennimalai, N., Dantzig, J.A., Jasiuk, I.M., 2012. Modeling of cortical bone
367 adaptation in a rat ulna: Effect of frequency. Bone 50(3), pp.792–797.

368 Lemaire, T., Lemonnier, S., Naili, S., 2012. On the paradoxical determinations of the lacuno-
369 canalicular permeability of bone. Biomechanics and Modeling in Mechanobiology, 11(7),
370 pp.933–946.

371 Lopez Franco, G.E., Blank, R.D., Akhter, M.P., 2011. Intrinsic material properties of cortical
372 bone. Journal of Bone and Mineral Metabolism, 29(1), pp.31–36.

373 Oyen, M.L., 2008. Poroelastic Nanoindentation Responses of Hydrated Bone. Journal of
374 Materials Research, 23(05), pp.1307–1314.

375 Oyen, M.L., Shean, T.A.V., Strange, D.G.T., Galli, M., 2012. Size Effects in Indentation of
376 Hydrated Biological Tissues. Journal of Materials Research, 27(01), pp.245–255.

377 Pereira, A.F. and Shefelbine, S.J., 2013. The influence of load repetition in bone
378 mechanotransduction using poroelastic finite-element models: the impact of permeability.
379 Biomechanics and Modeling in Mechanobiology.

380 Price, C., Zhou, X., Li, W., Wang, L., 2011. Real-Time Measurement of Solute Transport
381 Within the Lacunar-Canalicular System of Mechanically Loaded Bone: Direct Evidence for
382 Load-Induced Fluid Flow. Journal of Bone and Mineral Research, 26(2), pp.277–285.

383 Raghavan, M., Sahar, N.D., Kohn, D.H., Morris, M.D., 2012. Age-specific profiles of tissue-
384 level composition and mechanical properties in murine cortical bone. Bone, 50(4), pp.942–
385 953.

386 Rodriguez-Florez, N., Oyen, M.L., Shefelbine, S.J., 2013. Insight into differences in
387 nanoindentation properties of bone. Journal of the Mechanical Behavior of Biomedical
388 Materials 18, pp.90–99.

389 Robling, A.G., Hinant, F.M., Burr, D.B., Turner, C.H., 2002. Improved bone structure and
390 strength after long-term mechanical loading is greatest if loading is separated into short bouts.
391 Journal of Bone and Mineral Research, 17(8), pp.1545–1554.

392 Schneider, P., Stauber, M., Voide, R., Stampanoni, M., Donahue, L.R., Müller, R., 2007.
393 Ultrastructural properties in cortical bone vary greatly in two inbred strains of mice as
394 assessed by synchrotron light based micro- and nano-CT. Journal of Bone and Mineral
395 Research, 22(10), pp.1557–1570.

396 Schneider, P., Meier, M., Wepf, R., Müller, R., 2010. Towards quantitative 3D imaging of
397 the osteocyte lacuno-canalicular network. Bone 47(5), pp.848–858.

398 Smit, T.H., Huyghe, J.M., Cowin, S.C., 2002. Estimation of the poroelastic parameters of
399 cortical bone. Journal of Biomechanics, 35(6), pp.829–835.

400 Somerville, J.M., Aspden, R.M., Armour, K.E., Armour, K.J., Reid, D.M., 2004. Growth of
401 C57Bl/6 Mice and the Material and Mechanical Properties of Cortical Bone from the Tibia.
402 Calcified Tissue International, 74(5), pp.469–475.

Voide, R., Schneider, P., Stauber, M., van Lenthe, G.H., Stampanoni, M., Müller, R., 2011. The importance of murine cortical bone microstructure for microcrack initiation and propagation. Bone 49(6), pp.1186–1193.

Wang, L., Fritton, S.P., Cowin, S.C., Weinbaum, S., 1999. Fluid pressure relaxation depends upon osteonal microstructure: modeling an oscillatory bending experiment. Journal of Biomechanics, 32(7), pp.663–672.

Wang, X. and Ni, Q., 2003. Determination of cortical bone porosity and pore size distribution using a low field pulsed NMR approach. Journal of Orthopaedic Research, 21(2), pp.312–319.

Wang, L., Wang, Y., Han, Y., Henderson, S.C., Majeska, R.J., Weinbaum, S., Schaffler, M.B., 2005. In situ measurement of solute transport in the bone lacunar-canalicular system. Proceedings of the National Academy of Sciences of the United States of America, 102(33), pp.11911–11916.

Warden, S.J. and Turner, C.H., 2004. Mechanotransduction in the cortical bone is most efficient at loading frequencies of 5-10 Hz. Bone 34(2), pp.261–270.

Wen, D., Androjna, C., Vasanji, A., Belovich, J., Midura, R.J., 2010. Lipids and collagen matrix restrict the hydraulic permeability within the porous compartment of adult cortical bone. Annals of Biomedical Engineering, 38(3), pp.558–569.

Zhou, X., Novotny, J.E., Wang, L., 2008. Modeling fluorescence recovery after photobleaching in loaded bone: potential applications in measuring fluid and solute transport in the osteocytic lacunar-canalicular system. Annals of Biomedical Engineering, 36(12), pp.1961–1977.

CAPTIONS

Figure 1: Multi-scale porosity of cortical bone of a murine tibia from vascular (red big channels) to lacunar-canalicular (yellow dots and small channels) porosity.

Figure 2: Outline of the experimental setup for nanoindentation. The distal halves of the tibiae of three B6 mice of 2, 7 and 12 months were embedded in epoxy resin and tested submerged in distilled water. A minimum of ten indents where made on each sample.

Figure 3: Average and standard deviations of shear modulus (left) and Poisson's ratio (right) of B6 tibiae of 2, 7 and 12 months ($p<0.05$).

Figure 4: Intrinsic permeability as a function of age when indenting bone with a 238 μm radius tip ($p<0.05$).

Figure 5: Intrinsic permeability distribution as a function of age (2, 7 and 12 months) when indenting bone with a 238 μm (left) and 500 μm (right) radius tip ($p<0.05$).

Figure 6: Displacement-time (h-t) curves corresponding to two indentations on the same 12 month-old bone using the 500 μm sphere tip. Fitting the high-displacement curves result in permeability values in the order of 10^{-21} m^2, while low-displacement curves give values in the order of 10^{-24} m^2.

Figure 7: Nano-CT image of a 12 month-old tibia at a resolution of 0.6 μm/pixel. Pores of varying sizes relative to the indenter size are shown. The shaded areas correspond to the contact areas imposed by the indenter. The 238 μm tip imposed contact radii a ~ 7 μm, whereas the 500 μm tip imposed contact radii a ~ 11 μm.

Figure1
Click here to download high resolution image

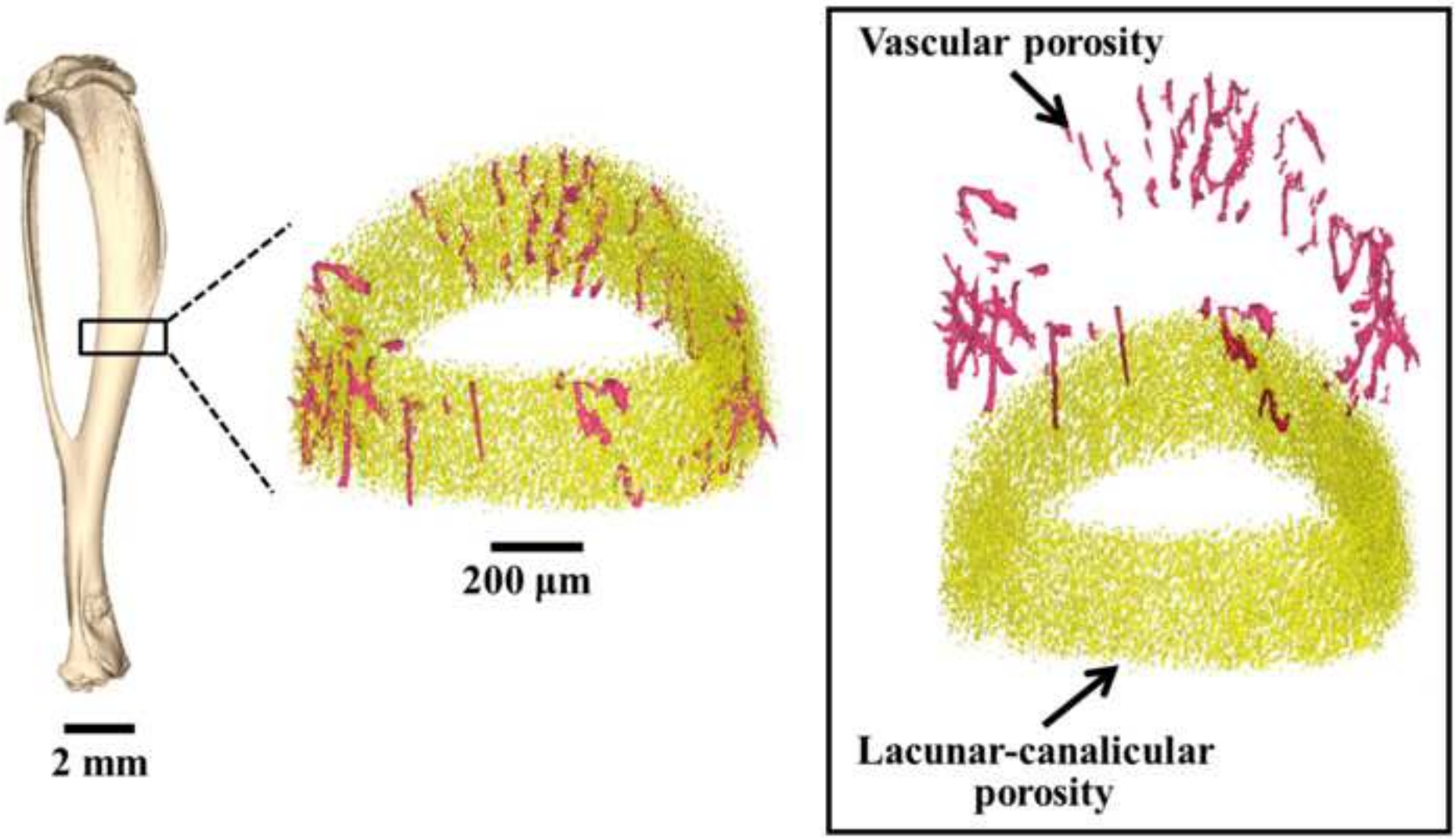

Figure2

Click here to download high resolution image

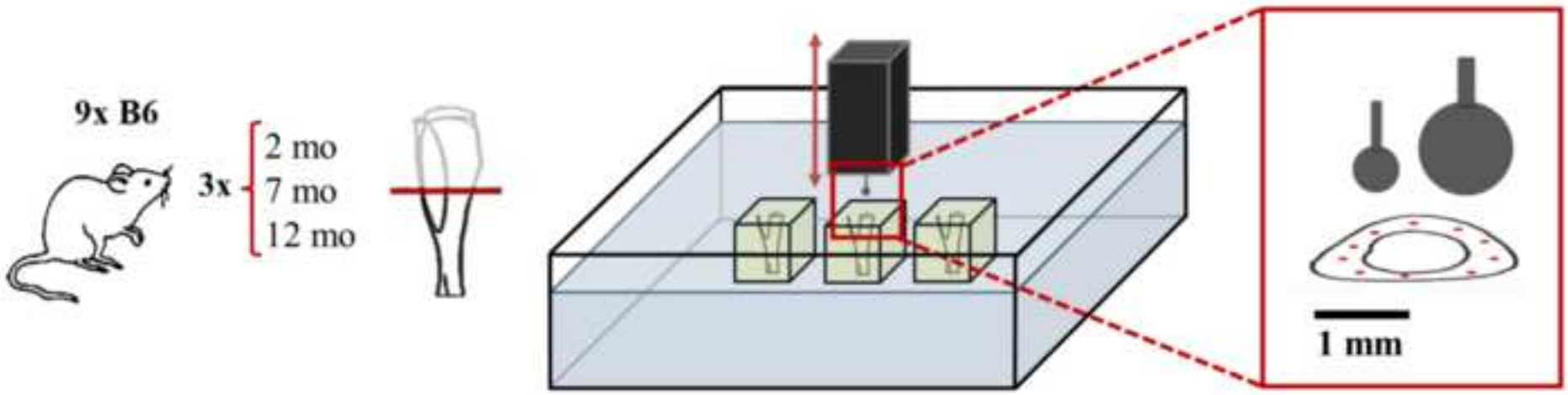

Figure3

Click here to download high resolution image

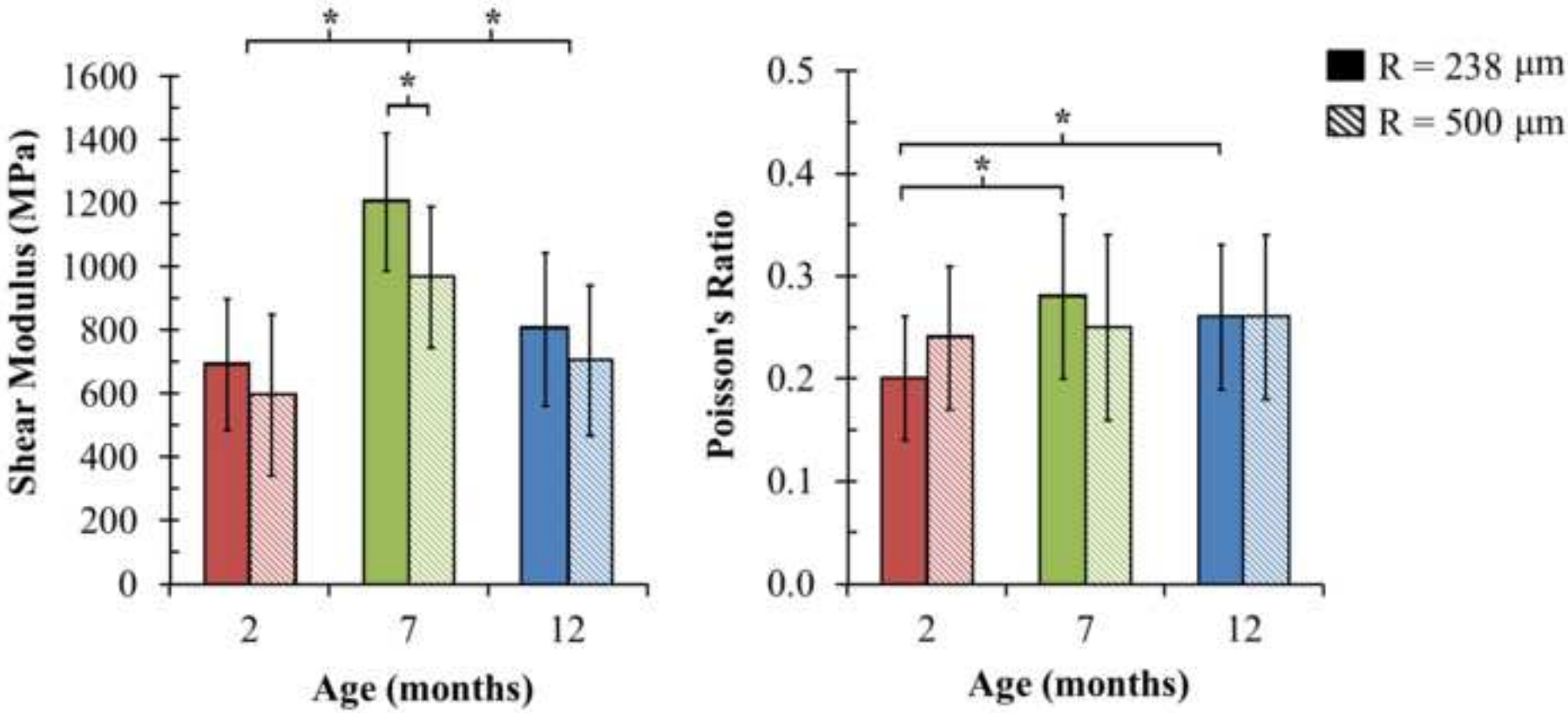

Figure4

Click here to download high resolution image

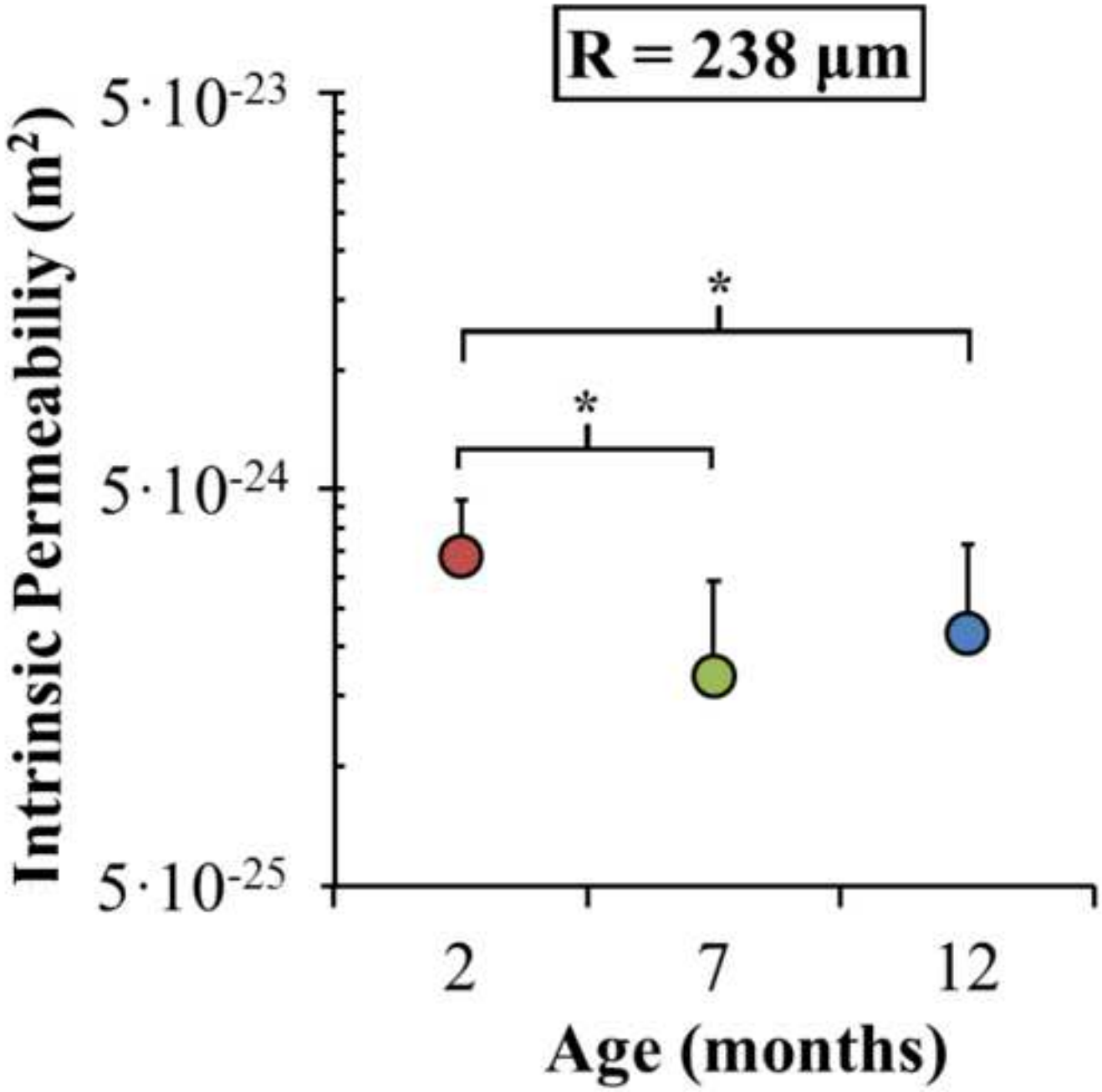

Figure5-revised

Click here to download high resolution image

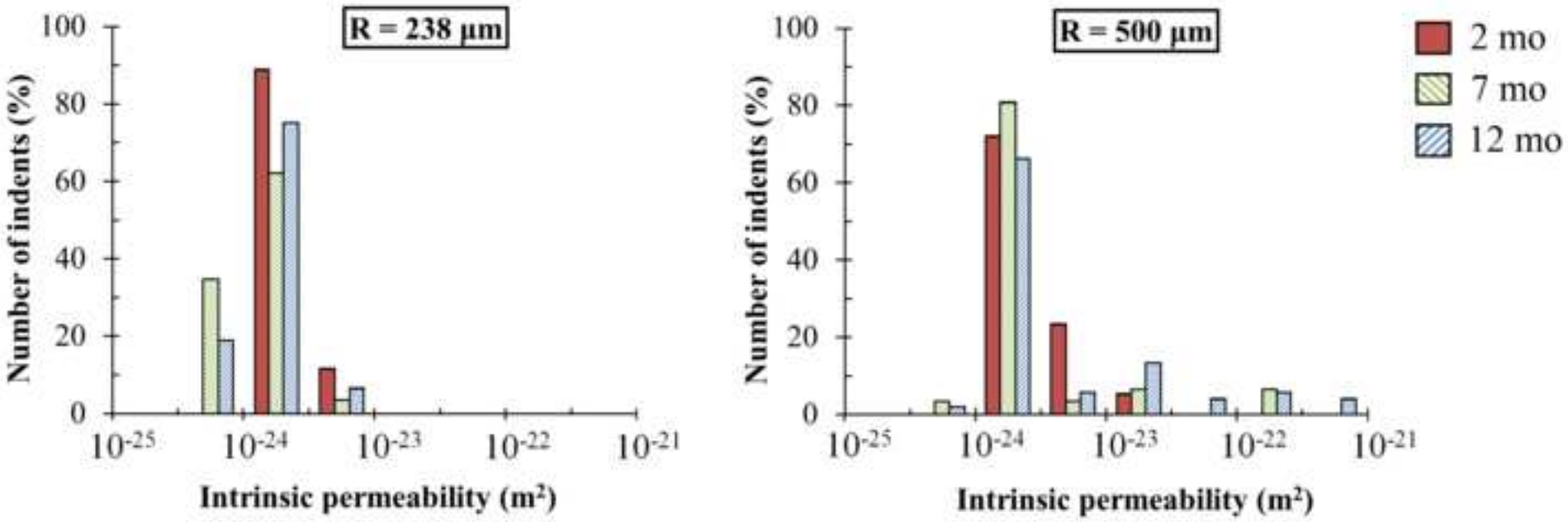

Figure6

Click here to download high resolution image

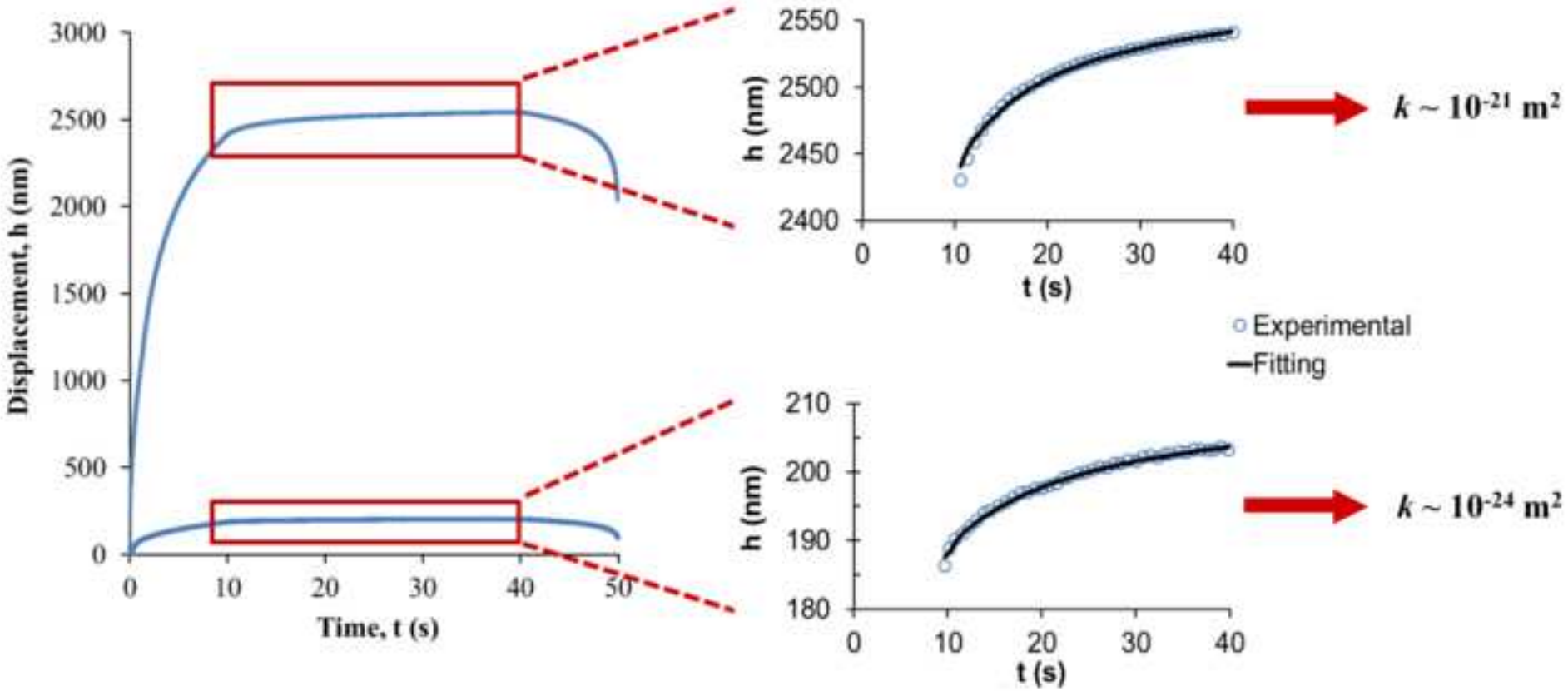

Figure7

Click here to download high resolution image